Counter-propagating wave acoustic particle manipulation device for the effective manufacture of composite materials.

Marc-S. Scholz, Bruce W. Drinkwater, Thomas M. Llewellyn-Jones, and Richard S. Trask

Abstract

An ultrasonic assembly device exhibiting broadband behaviour and a sacrificial plastic frame is described. This device is used to assemble a variety of microscopic particles differing in size, shape, and material into simple patterns within a number of host fluids. When the host fluid is epoxy the assembled materials can be cured and the composite sample extracted from the sacrificial frame. The wideband performance means that within a single device, the wavelength can be varied leading to control of the length scale of the acoustic radiation force field. We show that glass fibres of $50\,\mu$m length and $14\,\mu$m diameter can be assembled into a series of stripes separated by 100s of microns in a time of $0.3\,$s. Finite element analysis is used to understand the attributes of the device which control its wideband characteristics. The bandwidth is shown to be governed by the damping produced by a combination of the plastic frame and the relatively large volume of the fluid particle mixture. The model also reveals that the acoustic radiation forces are a maximum near the substrate of the device which is in agreement with experimental observations. The device is extended to 8-transducers and used to assemble more complex particle distributions.

Index Terms

Acoustic radiation pressure, Acoustophoretic force, Metamaterials, Particle manipulation, Ultrasonic assembly.

Manuscript received Thursday 9th April, 2015; revised.
The authors are with the University of Bristol, Queen's Building, University Walk, Bristol, BS8 1TR, United Kingdom.

Counter-propagating wave acoustic particle manipulation device for the effective manufacture of composite materials.

I. Introduction

Across a diverse range of applications, acoustic particle manipulation techniques have been employed to trap micron- to millimeter-size objects and to form ordered arrays of particles. The most common of these devices produce a standing wave between a transducer and a reflector (see reviews by Laurell *et al.* [1] and Evander *et al.* [2]) and have seen application, particularly in the biomedical field to, for example, tissue engineering [3], [4]. Devices with additional transducers have also been explored and shown to be able to create a wide range of patterns [5], [6], [7] and allow these patterns to be translated [8], [9], [10], [11].

An area of developing interest is the ultrasonic assembly of composite materials [12], [13], [14], [15], [16], [17], [18], [19] and the related areas of metamaterial manufacture [20], [21]. In addition to producing a particular distribution of particles the manufacture of a composite material requires the additional step of curing the host materials to create a solid. To date, although acoustic assembly of both spherical and fibrous particles in polymeric matrix media including acrylics, agar, epoxy, polyester, and polysiloxane has been shown to be possible, the repeatable manufacture of such specimens in an effective manner remains largely unexplored. For example, the removal of ultrasonically assembled composite samples from inside the devices manipulation cavity is often achieved only with great difficulty, due to chemical bonding of the polymer to its surroundings. Furthermore, previous particle manipulation devices typically operate at a limited number of specific resonant frequencies, thus limiting the number of predetermined patterns that can be formed by a single device [12], [13], [14], [15], [16], [20], [17], [18], [19], [21].

In this article, we aim to address the above issues and analyse the performance of a counter-propagating wave device designed specifically for the ultrasonic assembly of composites. Our device has a sacrificial plastic frame which simplifies sample extraction and operates across a broadband of frequencies making it flexible, in terms of the spacing of the particle distributions possible. This device then enables the fast and reliable fabrication of thin layers of anisotropic structural composite.

II. Ultrasonic device

The design forming the basis of investigation in this article, is shown in Fig. 1 and was previously described in [18]. Two opposed parallel $0.975\,\text{mm} \times 15\,\text{mm} \times 2\,\text{mm}$ lead zirconate titanate (PZT) transducers (Noliac NCE51) were separated from a central $30\,\text{mm} \times 15\,\text{mm} \times 2\,\text{mm}$ manipulation cavity by

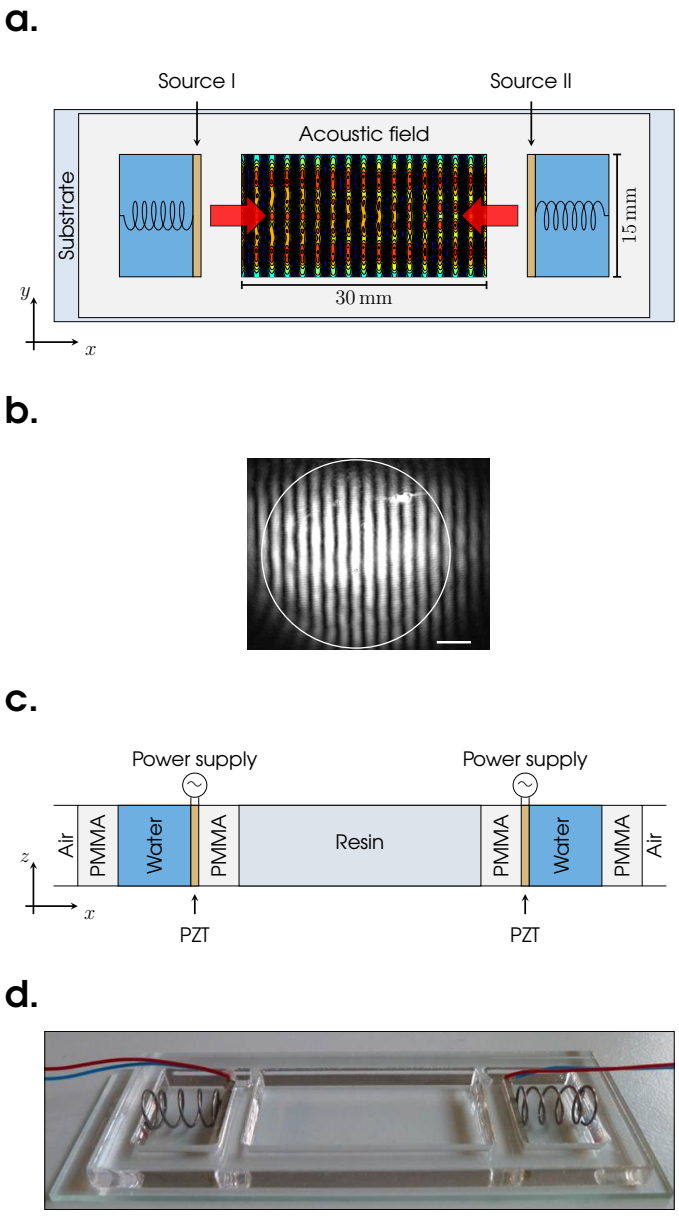

Figure 1: Two-element ultrasonic device. (a) A pair of opposed parallel PZT transducers generates an acoustic standing wave field inside the central cavity. (b) Schlieren image [22] from within the device's water filled central cavity at $\nu = 2.0\,\text{MHz}$. The image is grayscale, with black representing low pressure regions and white indicating maximum pressure. The scale bar measures 1 mm. (c) cross-sectional representation of the device by material layers: air (∞), PMMA (5 mm), H_2O (9.025 mm), PZT (0.975 mm), PMMA (5 mm), resin (30 mm), PMMA (5 mm), PZT (0.975 mm), H_2O (9.025 mm), PMMA (5 mm), air (∞). (d) photograph of the device.

a 5 mm thick poly(methyl methacrylate) (PMMA) boundary, which served to protect the acoustic system from the resin during polymerisation. The PMMA frame was treated as a sacrificial component and mounted on a glass microscope slide using double sided adhesive tape (tesa 64621-00007-01). Consequently, both piezoceramic plates could be recycled post matrix polymerisation. Two further cavities on either side of the device were filled with water to provide a heat sink at high driving voltages, $V_0 > 60\,\mathrm{V_{pp}}$. A small compression spring secured each transducer in its position by gently pressing it against the PMMA boundary. Typically, a driving voltage of $80\,\mathrm{V_{pp}}$ (at $\nu = 2\,\mathrm{MHz}$) was used to manipulate 50 µm (⌀14 µm) glass fibres, when suspended in a photocurable epoxy matrix with viscosity, $\eta \sim 0.3\,\mathrm{Pa\,s}$; in water ($\eta \sim 0.8 \times 10^{-3}\,\mathrm{Pa\,s}$), a voltage of $35\,\mathrm{V_{pp}}$ was found to be sufficient for a good quality pattern of well defined parallel lines to form, at the same frequency.

III. Experimental Methods and Results

A. Ultrasonic assembly

The device is able to ultrasonically assemble a variety of particles both spherical of radius, $a = 0.5\,\mu\mathrm{m} - 56\,\mu\mathrm{m}$ and cylindrical of length, $l = 50\,\mu\mathrm{m} - 750\,\mu\mathrm{m}$ and radius, $a = 2\,\mu\mathrm{m} - 7\,\mu\mathrm{m}$ into lines corresponding to pressure nodes within the central chamber. The spherical particles included polystyrene beads (Fig. 2 (a)), and microcapsules with a polyurethane (PU) or poly(urea-formaldehyde) (PUF) shell and a bisphenol A diglycidyl ether (DGEBA) core (Fig. 2 (b)), the cylindrical particles comprised of fibre reinforcements made from glass (Fig. 2 (c)), carbon (Fig. 2 (d)) and polycrystalline wool (PCW) (Fig. 2 (e)), and cellulose nanowhiskers [23] (Fig. 2 (f)).

The particles were found to align across a wide range of frequencies, centered around transducer resonances at 1.25 MHz, 1.97 MHz and 2.27 MHz - determined by electrical impedance analysis (in air). Experimental evidence of this wide band device behaviour is provided in Fig. 3.

Using a high speed video system (Photron, FASTCAM SA1), the particle assembly time of 50 µm (⌀14 µm) glass fibres in water was determined. With frames captured at a rate of $5000\,\mathrm{s^{-1}}$, full assembly was seen to be achieved within $t \sim 326\,\mathrm{ms} \pm 20\,\mathrm{ms}$ (obtained by manual inspection), at a frequency, $\nu = 2\,\mathrm{MHz}$ and a voltage, $V_0 = 38\,\mathrm{V_{pp}}$. In Fig. 4, a series of micrographs show the assembly process, with a movie file available as supplementary content.

While the majority of particles are seen to assemble into parallel lines, a few were seen to remain stationary and unaffected by the field. This is thought to be a consequence of frictional effects and secondary bonding, where particles are in direct contact with the glass substrate. It was noted that for an individual particle the time of travel from a position of maximum force ($\lambda/8$ away from a node) was generally below the global assembly time, $t \sim 326\,\mathrm{ms} \pm 20\,\mathrm{ms}$ at only $\sim 113\,\mathrm{ms} \pm 20\,\mathrm{ms}$ (obtained by manual inspection). In some cases, this was attributed to the proximity between a particle's origin and its final position at a pressure node. For other particles, however, a delay of the order of a few ms appeared to be observable before motion commenced. This could be the result of local inter-particle or frictional effects, becoming particularly pronounced in the presence of large numbers of fibres.

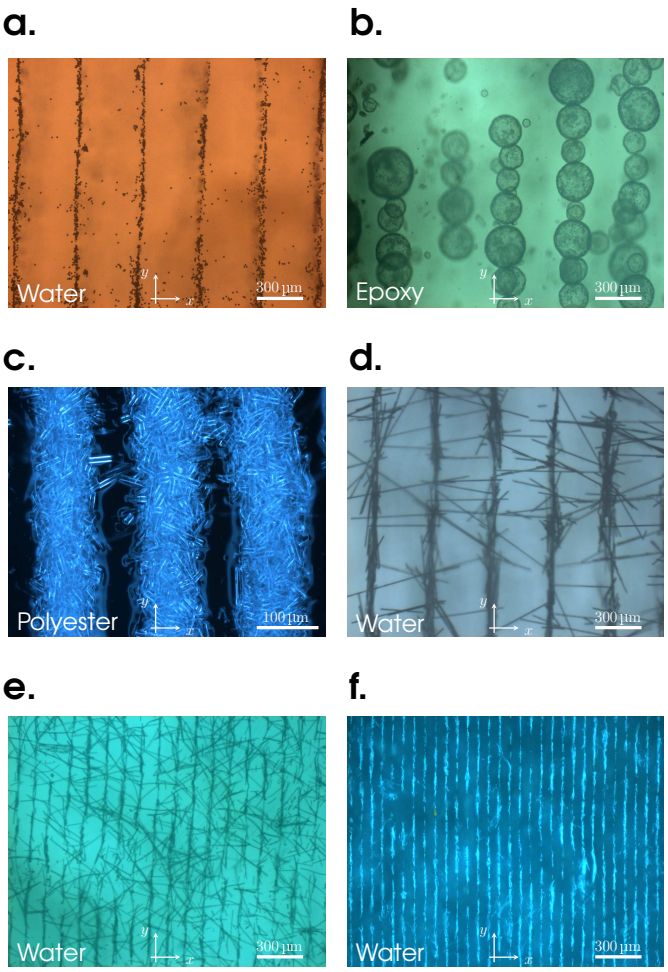

Figure 2: (a) ⌀10 µm polystyrene beads assembled in water at a separation $\lambda/2 = 368\,\mu\mathrm{m}$, (b) ⌀113 µm capsules made from a PU and PUF shell and an ethyl phenylacetate with dissolved DGEBA (9%) core assembled in an epoxy matrix at a separation $\lambda/2 = 368\,\mu\mathrm{m}$, (c) 50 µm (⌀14 µm) glass fibres aligned in a polyester matrix at a separation $\lambda/2 = 368\,\mu\mathrm{m}$, (d) 750 µm (⌀7 µm) carbon reinforcements aligned in water at a separation $\lambda/2 = 315\,\mu\mathrm{m}$, (e) 75 µm (⌀4 µm) PCW fibres aligned in water at a separation $\lambda/2 = 109\,\mu\mathrm{m}$, and (f) bundles of 1 µm cellulose nano-whiskers [23] distributed in water with a spacing of $\lambda/2 = 66\,\mu\mathrm{m}$.

For comparison, the global assembly time of ⌀10 µm polystyrene beads in water ($\nu = 2\,\mathrm{MHz}$, $V_0 = 38\,\mathrm{V_{pp}}$) was recorded as $t = 16.5\,\mathrm{s} \pm 0.2\,\mathrm{s}$, while the time of travel for an individual microsphere (starting at a position $\lambda/8$ from a node) was of the order of $\sim 667\,\mathrm{ms} \pm 200\,\mathrm{ms}$ (Fig. 5). Here, particle tracking software [24] could be employed (requires particles to be near spherical), and the global assembly could be quantified as the time taken for 95 % of particles to reach a nodal plane. It was noted that fewer particles remained stationary in this case, supporting the hypothesis that secondary bonds (at glass/glass interface) affected the experiment in the case of glass fibre particles.

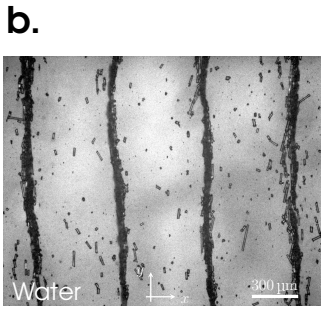

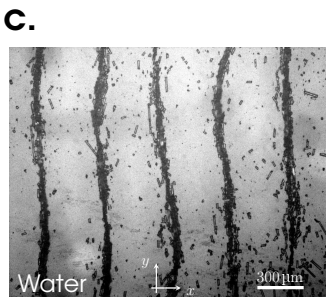

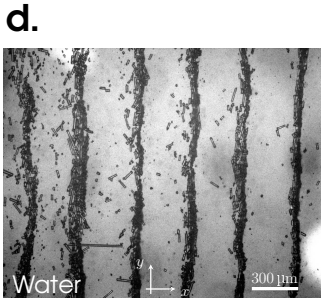

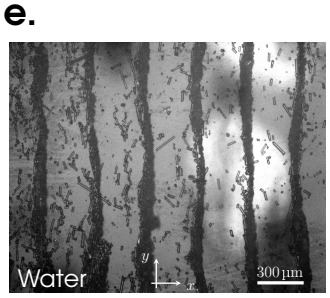

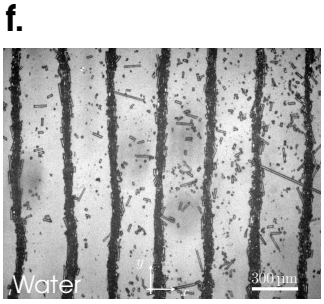

Figure 3: 50 µm (⌀14 µm) glass fibres assembled in water across a range of frequencies: (a) $\nu = 1.09$ MHz, (b) $\nu = 1.42$ MHz, (c) $\nu = 1.97$ MHz, (d) $\nu = 2.27$ MHz, (e) $\nu = 2.35$ MHz, and (f) $\nu = 2.50$ MHz.

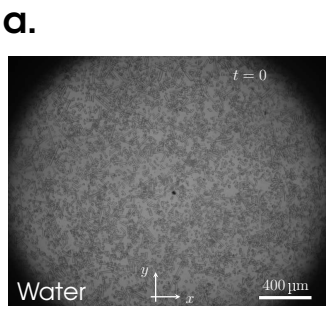

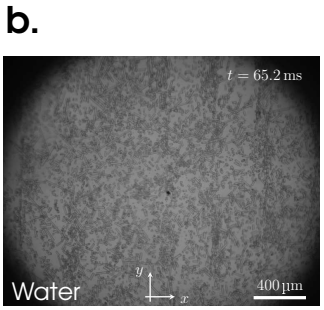

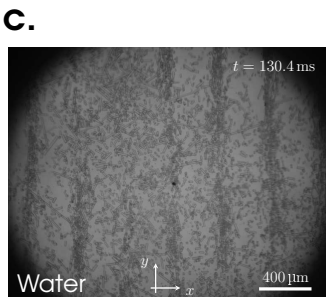

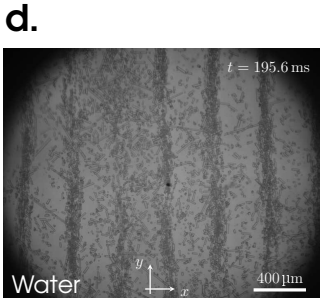

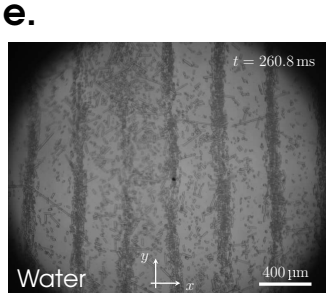

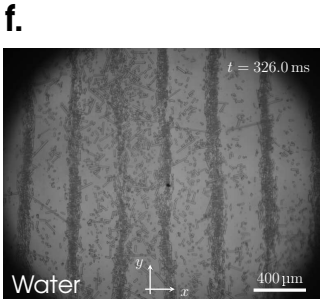

Figure 4: Ultrasonic assembly of short glass fibre particles (l = 50 µm, ⌀14 µm) dispersed in water, in the time domain with $\nu = 2$ MHz and $V_0 = 38\,V_{pp}$. Images were taken at a frame rate of $5000\,s^{-1}$ using an ultra high-speed video system (Photron, FASTCAM SA1.1). A movie file is available as supplementary material.

IV. Numerical acoustic modelling

A two-dimensional linear acoustic finite element model was used (COMSOL Multiphysics) to understand the device's acoustic response in relation to the individual physical and geometric attributes of the design. This approach is expected to accurately describe the device's resonant characteristics - more so than common one-dimensional transmission line analysis [25], [26], [27] - due to its ability to account for electro-acoustic coupling across two dimensions. In the following, it is assumed that the out-of-plane dimension (y-coordinate) is large compared to the wavelength, which is reasonable for the device depth $y = 15$ mm corresponding to 10.1 wavelengths at $\nu = 1$ MHz, taking $c = 1480\,m\,s^{-1}$.

A. Model development

The finite element model was set up using the *'Acoustic-Piezoelectric Interaction (acpz)'* interface [28], with geometric domains numbered sequentially from 1 to 10 as shown in Fig. 6 (a). Any material and domain parameters are listed in Table I; unless stated otherwise, these were applied throughout this section. The device's PMMA frame (domains 1, 4, 6, and 9) and glass substrate (domain 10) were treated as isotropic linear elastic solids, while the fluid domains (2, 5, and 8) were assigned the properties of water and said to behave as a linear elastic fluid with attenuation coefficient, $\alpha_{water} = 0.217{\cdot}\nu^2$ dB m^{-1} MHz^{-2} [29]. Any attenuation in the solid domains was specified in terms of the isotropic structural loss factor, $\tan\delta$ which may be expressed as

$$\tan\delta = \frac{1}{Q} = \frac{c\alpha}{\pi\nu}. \tag{1}$$

Here, the Q-factor was defined as a function of frequency by data extrapolation from [29], separately for PMMA and glass. A constant dielectric dissipation factor, $\tan\delta = 1/80$ was defined across the piezoelectric material domains 3 and 7 [30].

A near frictionless contact was simulated along the PZT/glass boundaries by means of a thin elastic layer with spring constants, $K_z = 1 \times 10^3\,N\,mm^{-1}$ specified in the z-direction (i.e. at normal to the boundary) and $K_x = 0$ acting along $\hat{x}$ (i.e. tangentially).

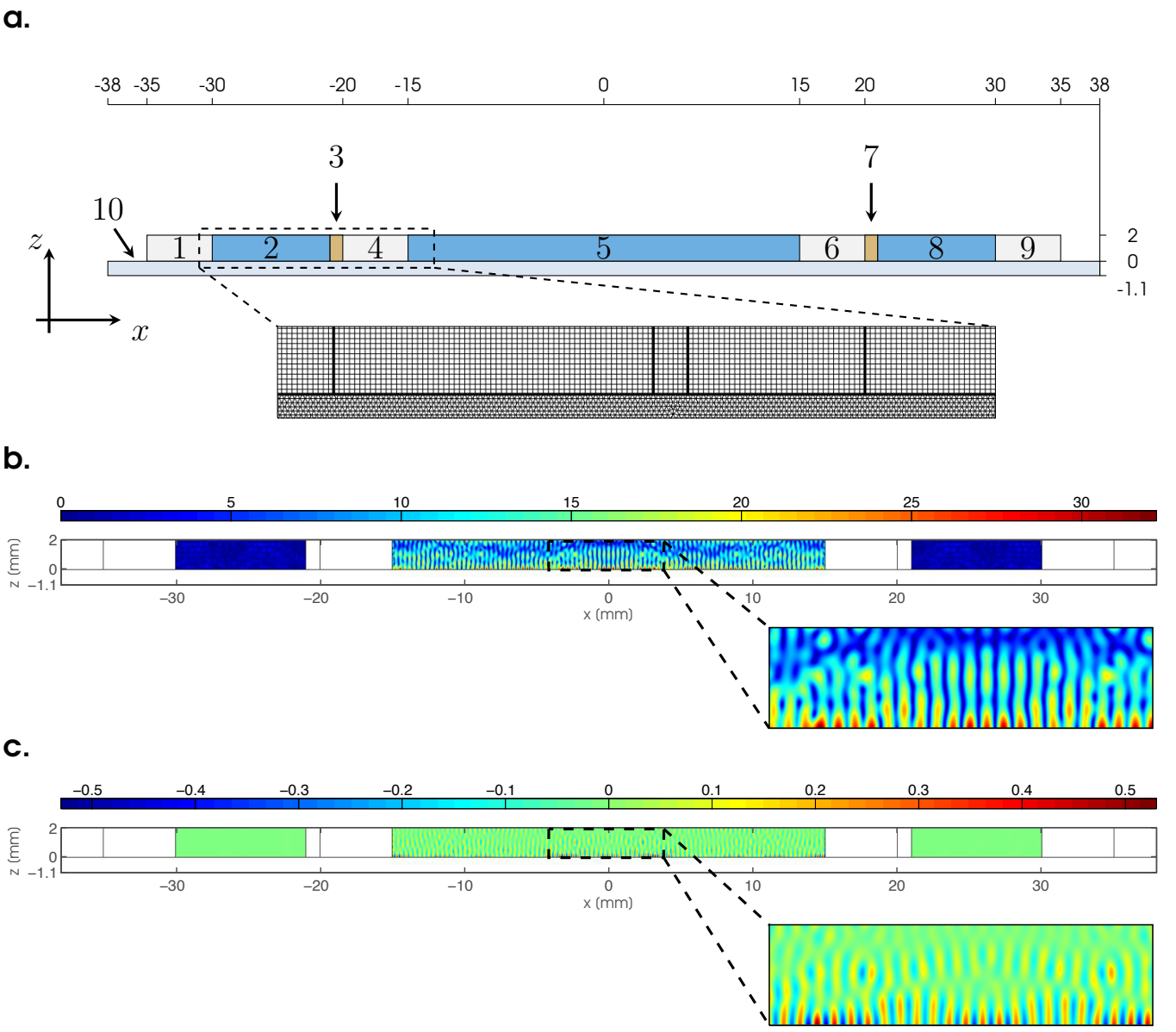

Figure 6: (a) Model geometry and mesh element distribution. Domains are labeled sequentially from 1 to 10. (b) Absolute acoustic pressure map at $\nu = 2.36\,\text{MHz}$, with $V_0 = 1\,\text{V}$. The pressure scale is in units of kPa with a maximum value of 32 kPa. (c) Acoustic force map (x-component) at $\nu = 2.36\,\text{MHz}$, with $V_0 = 1\,\text{V}$. The colour scale indicates force in units of pN with a minimum value of $-0.53\,\text{pN}$ and a maximum value of $0.53\,\text{pN}$. All forces are calculated using (2) and for a $\varnothing 10\,\mu\text{m}$ spherical polystyrene particle in water.

Each PZT transducer (domains 3 and 7) had a sinusoidal electric potential of amplitude, $V_0 = 1\,\text{V}$ applied to its forward facing boundary, with a ground condition specified at the back. All remaining PZT boundaries were assigned zero charge.

The interaction of fluid (2, 5, and 8) and solid (1, 3, 4, 6, 7, 9, and 10) domains was accounted for by defining an acoustic-structure boundary [28] along any fluid to solid interfaces. A sound hard boundary circumscribing the model reflected any waves reaching the geometry's bounding edges.

As is indicated in Fig. 6, a mesh was constructed from a combination of triangular (domain 10) and mapped rectangular (domains 1 to 9) elements. The element size was set globally to $\leq \lambda/10$, a value confirmed to be sufficiently small for the model to converge.

Finally, an out-of-plane thickness parameter was set at 15 mm; this is required by COMSOL, as intensive physical quantities are specified independent of space dimension (e.g. density in units of $\text{kg}\,\text{m}^{-3}$), and in this case must be reduced to planar 2D.

The model was solved in the frequency domain, using the default stationary solver configuration. On a standard desktop computer, the calculation time for a single frequency was between 1 s and 23 s. With the maximum number of degrees of freedom of the order of $\sim 4.6 \times 10^5$, the model was highly memory intensive, requiring as much as 19 GB RAM to solve for 257 frequency points in the range $1.0\,\text{MHz} \leq \nu \leq 2.5\,\text{MHz}$.

Table I: Baseline parameters. Ref.: Reference.

Material	Domains	Parameter	Value	Ref.
Glass	10	Density	$2600\,\mathrm{kg\,m^{-3}}$	[29]
		Longitudinal wavespeed	$5570\,\mathrm{m\,s^{-1}}$	[29]
		Shear wavespeed	$3430\,\mathrm{m\,s^{-1}}$	[29]
		Q-factor, 1.0 MHz	67	[29]
		2.5 MHz	72	
PMMA	1,4,6,9	Density	$1190\,\mathrm{kg\,m^{-3}}$	[29]
		Longitudinal wavespeed	$2700\,\mathrm{m\,s^{-1}}$	[29]
		Shear wavespeed	$1100\,\mathrm{m\,s^{-1}}$	[29]
		Q-factor, 1.0 MHz	2450	[29]
		2.5 MHz	2041	
PZT	3,7	Density	$7850\,\mathrm{kg\,m^{-3}}$	[30]
		Longitudinal wavespeed	$4500\,\mathrm{m\,s^{-1}}$	[30]
		Q-factor	80	[30]
Water	2,5,8	Density	$1000\,\mathrm{kg\,m^{-3}}$	-
		Longitudinal wavespeed	$1480\,\mathrm{m\,s^{-1}}$	[29]
		Attenuation coefficient	$0.217 \cdot \nu^2\ \mathrm{dB\,m^{-1}\,MHz^{-2}}$	[29]
		Dynamic viscosity	$1 \times 10^{-3}\,\mathrm{Pa\,s}$	[31]
Air	2,8	Density	$1.20\,\mathrm{kg\,m^{-3}}$	-
		Longitudinal wavespeed	$344\,\mathrm{m\,s^{-1}}$	[29]
		Attenuation coefficient	$170 \cdot \nu^2\ \mathrm{dB\,m^{-1}\,MHz^{-2}}$	[29]
Polystyrene	Particle	Radius	5 µm	-
		Density	$1100\,\mathrm{kg\,m^{-3}}$	[29]
		Longitudinal wavespeed	$2670\,\mathrm{m\,s^{-1}}$	[29]

B. Acoustic pressure distribution

First, the electrical input impedance was extracted and compared to experimental data. A good correspondence was achieved across the frequency range $1.0\,\mathrm{MHz} \leq \nu \leq 2.5\,\mathrm{MHz}$, as can be seen from Fig. 7 (a). Some additional sensitivity to frequency was seen in the simulation, suggesting that the model was more lightly damped than reality. However, the model still clearly captures much of the experimentally observed behaviour both quantitatively and qualitatively.

An evaluation of the maximum acoustic pressure in the manipulation cavity (Fig. 7 (b)) found there to be four distinctly defined regions of high pressure. By fitting a six-term Fourier series [32] to smooth the data, these may be defined in terms of local maxima at $\nu = 1.27\,\mathrm{MHz}$ (A), $\nu = 1.64\,\mathrm{MHz}$ (C), $\nu = 2.00\,\mathrm{MHz}$ (E), and $\nu = 2.36\,\mathrm{MHz}$ (G) with corresponding pressures, $p_1 = 26\,\mathrm{kPa}$, $p_2 = 16\,\mathrm{kPa}$, $p_3 = 41\,\mathrm{kPa}$, and $p_4 = 36\,\mathrm{kPa}$. At the first, third and fourth maxima, a frequency bandwidth could further be estimated as the full width at half maximum (FWHM), giving $w_1 = 0.32\,\mathrm{MHz}$, $w_3 = 0.26\,\mathrm{MHz}$, and $w_4 = 0.24\,\mathrm{MHz}$.

To explore the theoretical and experimentally observed broadband characteristics further, the acoustic pressure distribution in the manipulation cavity was measured as a function of frequency. A needle hydrophone (Precision Acoustics) with a $\varnothing 0.5\,\mathrm{mm}$ probe was used to measure the maximum time averaged pressure along a line $-3.6 \leq x \leq 3.6$ at the center of the device ($y = 0$), where each measurement was taken over a time interval of $25\,\mu\mathrm{s}$ and at a step size, $\delta x = 0.3$. On taking the fast Fourier transform of the time domain signal, and scanning across a frequency range $1.0\,\mathrm{MHz} \leq \nu \leq 2.5\,\mathrm{MHz}$ the result shown in Fig. 7 (c) was obtained. The size of the needle hydrophone (with the probe diameter, $s \sim 0.34\lambda$ at $1\,\mathrm{MHz}$ and $s \sim 0.84\lambda$ at $2.5\,\mathrm{MHz}$) in relation to the wavelength and the pressure variability in the z-direction (see Fig. 6 (b)) meant that the measured pressure could not be quantitatively compared to the simulations. However, the measured pressure was normalised and is included here to show additional evidence of the broadband behaviour of the device. We note that as in Fig. 7 (c) four pressure peaks could again be identified by fitting a six-term Fourier series to smooth the data. Pressure maxima were found at $\nu = 1.23\,\mathrm{MHz}$, $\nu = 1.58\,\mathrm{MHz}$, $\nu = 1.78\,\mathrm{MHz}$, and $\nu = 2.27\,\mathrm{MHz}$, for the first of which a frequency bandwidth (FWHM) of $w_{1'} = 0.20\,\mathrm{MHz}$ could be calculated. On comparison with the location of the pressure peaks as predicted by the model, a deviation of $\pm 2\,\%$, $\pm 3\,\%$, $\pm 10\,\%$, and $\pm 4\,\%$ was observed from the frequencies of A, C, E and G, respectively. All experimentally measured pressure maxima lay well within the corresponding predicted bandwidths, w_1 to w_4. Finally, it is worth noting that the theoretically predicted maximum pressure along a line $z = 0.3\,\mathrm{mm}$ agreed with the experimentally measured pressure to within $\pm 12\,\mathrm{kPa}$ in the low frequency region, where $1.0\,\mathrm{MHz} \leq \nu \leq 1.3\,\mathrm{MHz}$.

As well as the pressure distribution as a function of frequency, a two-dimensional pressure map could be extracted from the model; an example is shown in Fig. 6 (b) for $\nu = 2.36\,\mathrm{MHz}$ and $V_0 = 1\,\mathrm{V}$. As expected, pressure nodes appeared equally spaced at intervals of $\lambda/2$ near the surface of the device's glass substrate. With increasing distance from

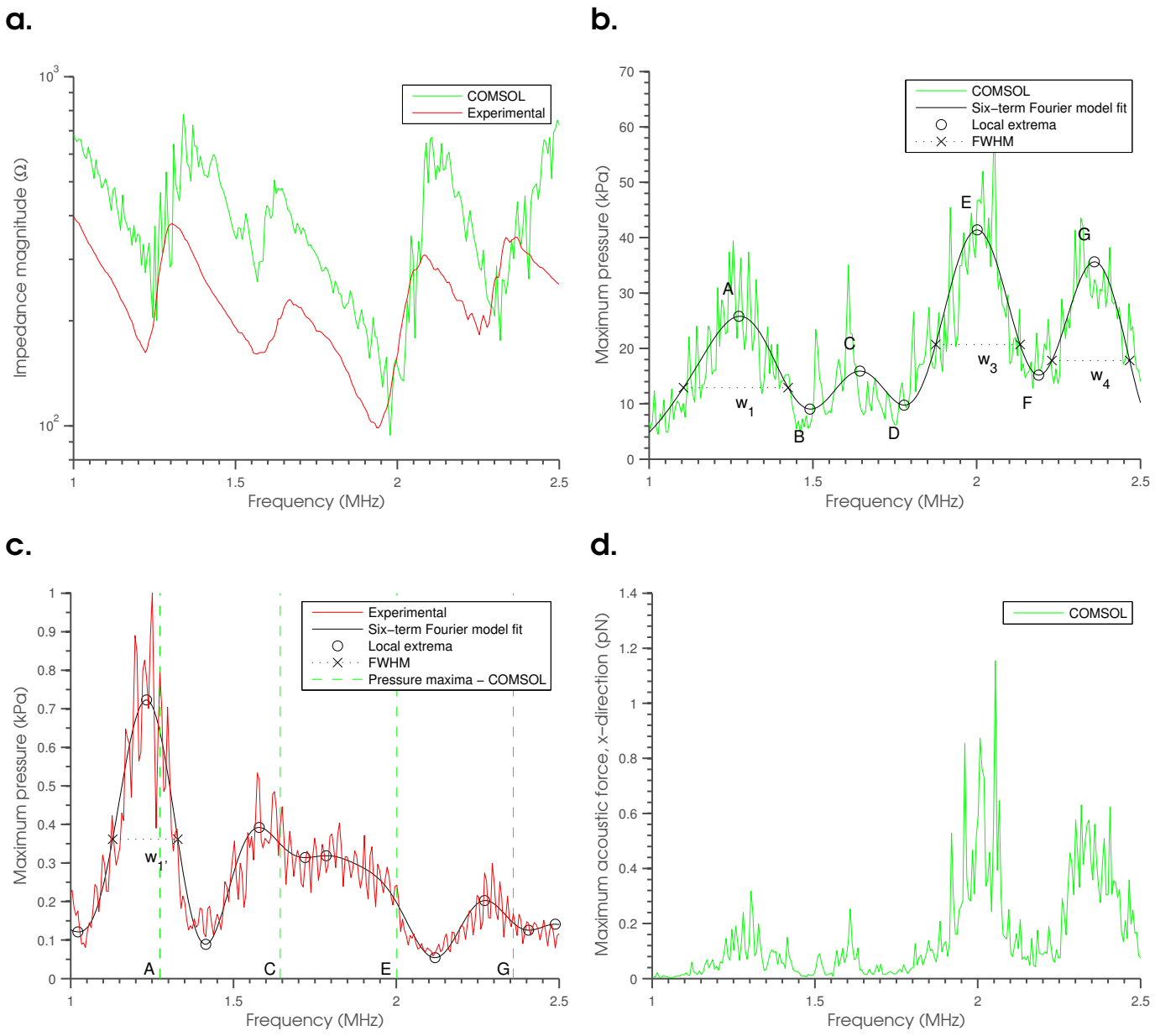

Figure 7: (a) Electrical input impedance at $V_0 = 1\,\mathrm{V}$, (b) predicted maximum acoustic pressure as a function of frequency for the range $1.0\,\mathrm{MHz} \leq \nu \leq 2.5\,\mathrm{MHz}$ ($V_0 = 1\,\mathrm{V}$), where the acoustic pressure bandwidth is calculated by estimation of the full width at half maximum (FWHM) at the first, $w_1 = 0.34\,\mathrm{MHz}$, third $w_3 = 0.27\,\mathrm{MHz}$, and fourth $w_4 = 0.25\,\mathrm{MHz}$ peak, (c) normalised acoustic pressure as determined experimentally, (d) predicted maximum acoustic force ($V_0 = 1\,\mathrm{V}$) on a $\varnothing 10\,\mu\mathrm{m}$ spherical polystyrene particle in water.

the substrate (where $z = 0$), however, a less clearly defined pattern of lines was observed. This finding is in agreement with the observation that the device best operates with particles assembling near the bottom of its central fluid cavity. This means that the device is more suitable for the manipulation of particles that are denser than the surrounding host medium (i.e. $\rho_p/\rho_0 > 1$) and hence accumulate on or near the substrate.

The dependence of the frequency sensitivity of the device on geometric parameters was studied (1) by changing the thickness of the PMMA boundary layers (domains 4 and 6) across a range from 2 mm to 7 mm (Fig. 8 (a)), and (2) by altering the central cavity (domain 5) dimensions between 1 mm and 30 mm (Fig. 8 (b)). On comparison of the traces of Fig. 8 (a), it is clear that the introduction of a PMMA boundary ahead of the transducer front face is largely responsible for the broadband characteristics of the present device. Much more sharply defined resonance peaks were found to be present in the frequency distribution of a device whose PMMA boundary is thin. This finding shows that the PMMA frame serves two purposes; (1) it acts as a sacrificial barrier simplifying sample extraction, and (2) adds damping to the acoustic system making it less sensitive to the chamber resonances. This latter property is particularly useful as it allows trapping to be maintained as the chamber resonances shift with temperature and during polymerisation of the host matrix. Similarly but to a lesser extent, the device performance was found to be

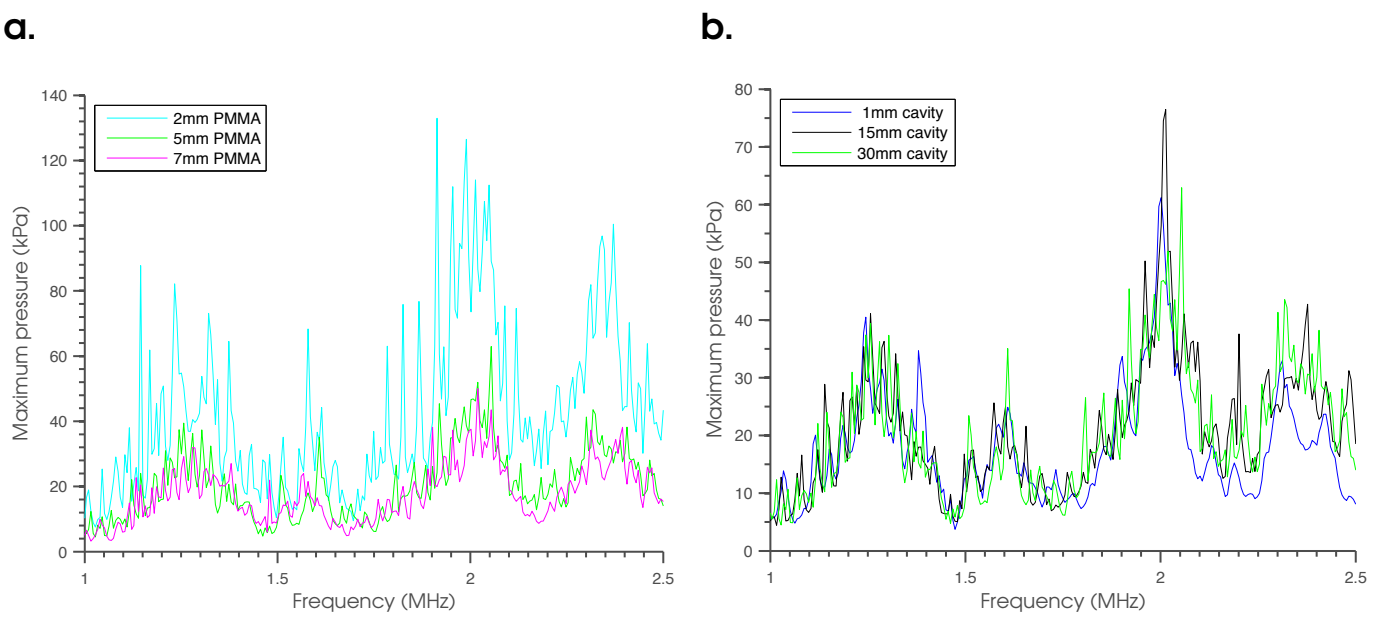

Figure 8: (a) Maximum acoustic pressure as a function of frequency for devices with a PMMA boundary thickness (domains 4 and 6) of 2 mm, 5 mm, and 7 mm. (b) Maximum acoustic pressure as a function of frequency for devices with cavity dimensions (domain 5) of 1 mm, 15 mm, and 30 mm but constant PMMA boundary thickness of 5 mm.

dependent on geometric design features for a device with smaller central chamber as can been seen from Fig. 8 (b).

C. Acoustophoretic force and assembly time

The theoretical maximum acoustophoretic force, F_{rad} on an isolated $\varnothing 10\,\mu\text{m}$ polystyrene sphere in water was found using the Gor'kov equation [33]:

$$F_{\text{rad}} = -2\pi a^3 \nabla \left[\frac{1}{3} f_1 \kappa_0 \langle p_{\text{in}}^2 \rangle - \frac{1}{2} f_2 \rho_0 \langle v_{\text{in}}^2 \rangle \right], \tag{2}$$

where

$$f_1 = 1 - \frac{\kappa_p}{\kappa_0}, \tag{3}$$

$$f_2 = \frac{2\left(\frac{\rho_p}{\rho_0} - 1\right)}{2\frac{\rho_p}{\rho_0} + 1}, \tag{4}$$

a is the particle radius, κ_0 and κ_p are the fluid and particle compressibilities, and ρ_0 and ρ_p are the density of the fluid and the particle, respectively. $\langle p_{\text{in}}^2 \rangle$ and $\langle v_{\text{in}}^2 \rangle$ are the time averaged squared sound pressure and velocity.

As expected from the predicted pressure distribution (Fig. 7 (b), Section IV-B), four broad peaks of maximum acoustic force could be identified across the previously discussed frequency bands; this is shown in Fig. 7 (d). A two-dimensional map of the predicted acoustic force on a $\varnothing 10\,\mu\text{m}$ spherical polystyrene particle in water is shown in Fig. 6 (c). Expectedly, a similar pattern of zero force and high force parallel lines (compared to low and high pressure regions in Fig. 6 (b)) extend along the x-direction in the central device cavity. It can be seen that these force lines decrease rapidly above $z > 0.3\,\text{mm}$, suggesting that the manipulation capability is mainly in this near-surface region.

From Fig. 7 (d), the theoretical acoustic force magnitude at $\nu = 2\,\text{MHz}$ ($V_0 = 1\,\text{V}$) acting on a $\varnothing 10\,\mu\text{m}$ spherical polystyrene particle is $0.89\,\text{pN}$. At $V_0 = 38\,\text{V}_{\text{pp}}$ a value of $0.32\,\text{nN}$ was extracted, which may be used to predict the approximate particle assembly time of an isolated particle; a measure of this quantity was previously obtained experimentally in Section III-A. A simple dynamic model can be developed in which a sinusoidal pressure field is assumed. If a node exists at $x = 0$ the equation of motion may be written in terms of the mass of the particle, $m = 4\rho_p \pi a^3/3$ the excitation force, F_0 the wavelength in the fluid, λ and the dynamic viscosity, μ of the fluid:

$$0 = m\ddot{x} + F_0 \sin\left(\frac{2\pi x}{\lambda}\right) + 6\pi\mu a\dot{x}. \tag{5}$$

The analytical solution to (5) is given - for an overdamped system - by Courtney *et al.* [6] as

$$x\,(t) = \frac{\lambda}{2\pi} \arctan\left[\tan\left(\frac{2\pi x_0}{\lambda}\right) e^{-\frac{2F_0 t}{3\lambda\mu a}}\right], \tag{6}$$

which is evaluated using an estimation of $F_0 = 0.32\,\text{nN}$ to give the displacement path shown in Fig. 9. Here, $x_0 = \lambda/8$ is the position of the particle at time $t = 0$, assuming the particle initially experiences a maximum acoustic force. At the experimentally determined individual assembly time, $t \sim 667\,\text{ms} \pm 200\,\text{ms}$ (6) predicts the particle to be a distance $x\,(667\,\text{ms}) = 1.8 \times 10^{-15}\,\mu\text{m}$ from a nodal position. However, it is clear from Fig. 9 that the particle arrives in the vicinity of the node in around 100 ms. This difference is thought to arise from a combination of the presence of friction in the experiment, an underestimate of the damping in the simulation, and the inherent variability of this force with both frequency (Fig. 7 (d)) and precise location (Fig. 6 (c)). Good agreement

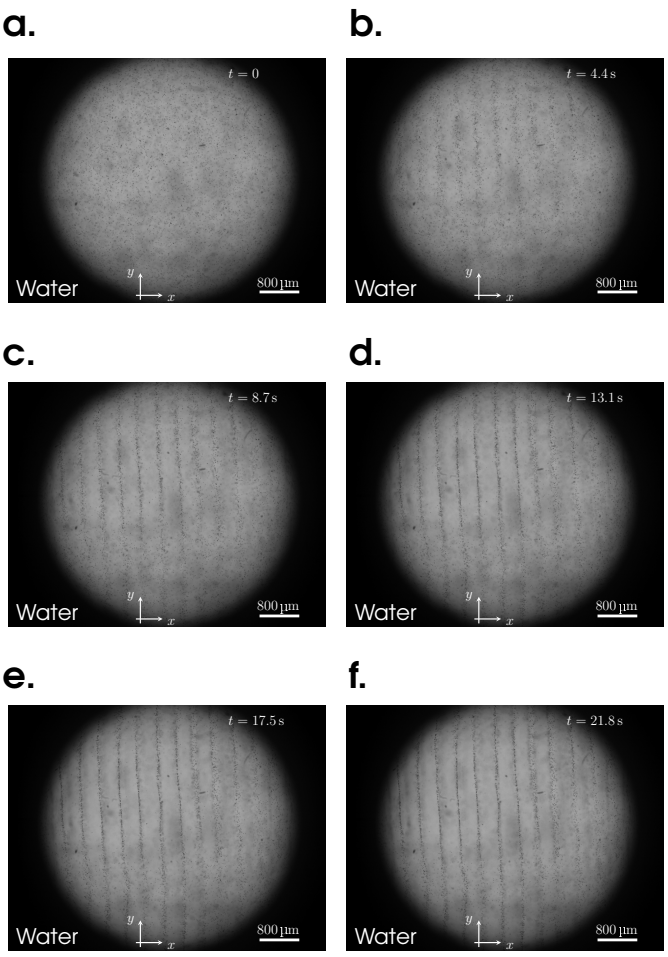

Figure 5: Translational motion of $\varnothing 10\,\mu$m dispersed in water, in the time domain with $\nu = 2\,$MHz and $V_0 = 38\,V_{pp}$. Images were taken at a frame rate of $250\,s^{-1}$ using an ultra high-speed video system (Photron, FASTCAM SA1.1). A movie file is available as supplementary material.

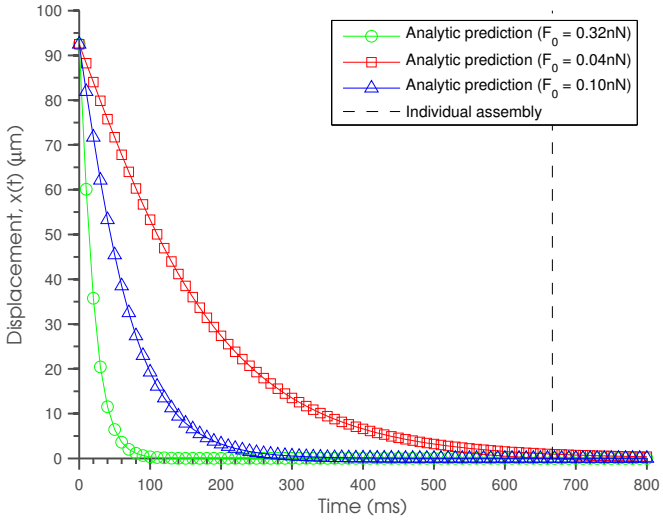

Figure 9: Particle assembly time calculated for a $\varnothing 10\,\mu$m spherical polystyrene particle in water. Initially, the particle is assumed to be at a position $x(0) = \lambda/8$, where the acoustic force is a maximum. Analytical predictions are the solution to (6). An experimental value for the assembly time of a single particle is also indicated around $t \sim 667\,\text{ms} \pm 200\,\text{ms}$.

with the experimentally found assembly time is obtained using an effective force, $F_0 = 0.04\,$nN, as can be seen in Fig. 9.

V. Ultrasonic Assembly with an Eight Element Array

In Sections II-IV, the discussion focused on the broadband frequency characteristics of the design from Fig. 1. Here, we give a brief account of how to extend the two transducer system to a more versatile eight transducer polygon of similar acoustic properties. The addition of further transducer elements primarily enables a more flexible control over the acoustic field as can be seen from Fig. 10; In Fig. 10 (a), a honeycomb-like formation of cylindrical particles was achieved on operation of two orthogonal pairs of opposed transducers; Fig. 10 (b) shows a staggered offset of small particle agglomerates that was formed by combining two pairs of opposed transducers at an angle of 45° to each other, with the horizontally aligned elements driven at an advancing phase of $\pi/2$. A more detailed discussion on the particle assembly patterns that can be generated using an octagonal acoustic particle manipulation device was previously given by Bernassau *et al.* [8], [7]. Importantly here, the broadband frequency characteristics of the two transducer model are maintained and the build time of the eight transducer device remains comparable. The device shown in Fig. 10 further adds the capability to use more intricate particle arrangements in conjunction with the ultrasonic assembly process of composite material structures. Specifically, the controlled positioning and alignment of short fibres within a matrix have the potential for composite structures with the properties of conventional fibre composites to be manufactured via additive layer manufacture.

VI. Conclusions

In conclusion, a counter-propagating acoustic wave device was shown to be suitable for the efficient manufacture of thin layers of anisotropic composite and was explored and shown to exhibit broad frequency band characteristics. Ultrasonic assembly was achieved across a range of particle materials, sizes and shapes as well as a variety of different fluid hosts (including water, epoxy, and polyester). Assembly times were observed to be of the order of a few hundred ms and a distinction was made between the time to node for a single particle and the time for all particles to assemble into the desired pattern. An in-depth study of the device's resonant behaviour was conducted in COMSOL and was able to predict the electrical input impedance, maximum acoustic pressure and acoustic force to a reasonable accuracy, not only in the vicinity of through thickness resonance modes of the transducer but also for two-dimensionally coupled flexural modes. The model identified four wideband frequency regions, across which ultrasonic assembly was also observed experimentally. This was attributed primarily to the presence of a PMMA barrier ahead of the transducer, introducing additional damping to the overall acoustic system. From analysis of the two-dimensional force distribution, areas of high force were found to be near the device's substrate surface. Finally, an extension of the device concept to a more versatile eight-element array

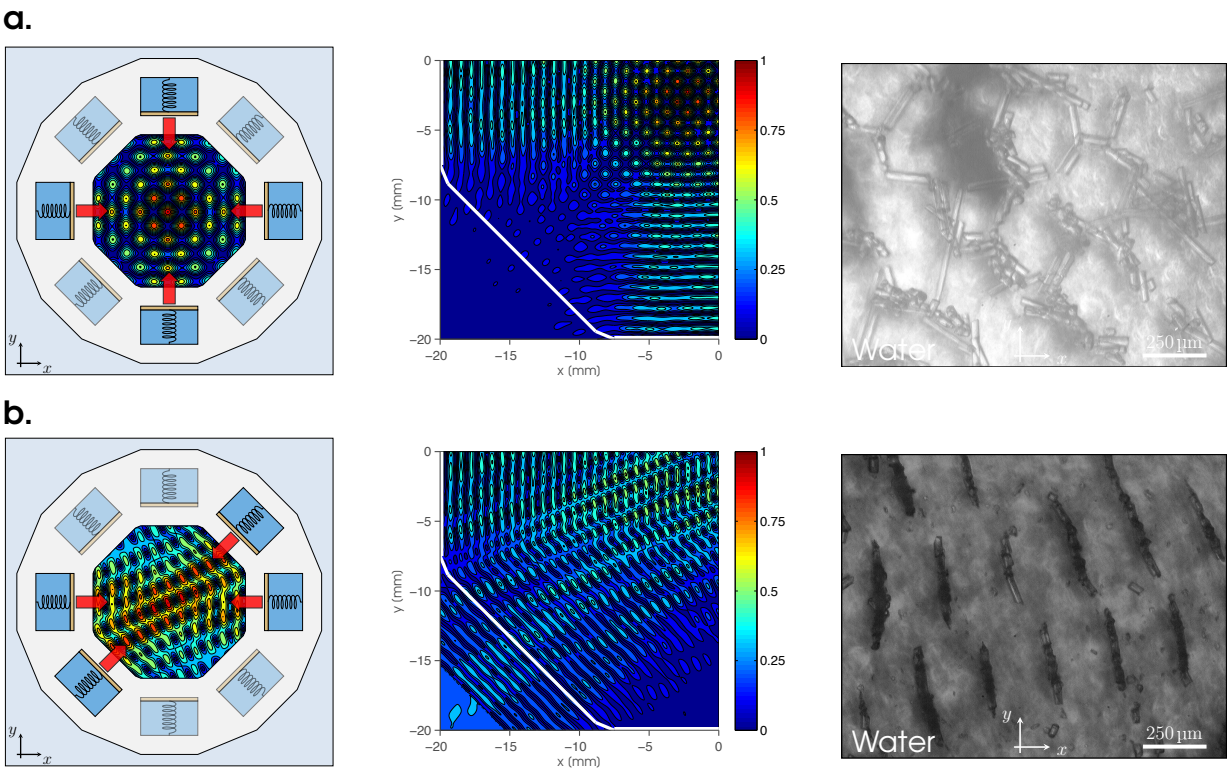

Figure 10: From left to right: active acoustic elements, a quarter model of the normalised acoustic pressure inside the manipulation cavity with a white solid line indicating the cavity border, experimentally observed assembly pattern formed by 50 µm (⌀14 µm) glass fibres. (a) An orthogonal arrangement of four transducers driven in-phase, (b) two pairs of opposed transducers making an angle of 45° where the horizontally aligned elements are driven at an advancing phase of $\pi/2$.

of similar characteristic acoustic behaviour was outlined. Here, the generation of more intricate particle assembly patterns is thought to be particularly relevant to the additive layer manufacture of short fibre reinforced composite structures.

ACKNOWLEDGMENT

The authors gratefully acknowledge funding from the EPSRC under its grants for the ACCIS Doctoral Training Centre (no. EP/G036772/1), and Engineering Fellowships for Growth (no. EP/M002489/1).

REFERENCES

[1] T. Laurell, F. Petersson, and A. Nilsson, "Chip integrated strategies for acoustic separation and manipulation of cells and particles," *Chem. Soc. Rev.*, vol. 36, pp. 492–506, 2007.

[2] M. Evanderl and J. Nilsson, "Acoustofluidics 20: Applications in acoustic trapping," *Lab Chip*, vol. 12, pp. 4667–4676, 2012.

[3] F. Gesellchen, A. Bernassau, T. Dejardin, D. Cumming, and M. Riehle, "Cell patterning with a heptagon acoustic tweezer - application in neurite guidance," *Lab Chip*, vol. 14, pp. 2266–2275, 2014.

[4] S. Li, P. Glynne-Jones, O. Andriotis, K. Ching, U. Jonnalagadda, R. Oreffo, M. Hill, and R. Tare, "Application of an acoustofluidic perfusion bioreactor for cartilage tissue engineering," *Lab Chip*, vol. 14, pp. 4475–4485, 2014.

[5] S. Oberti, A. Neild, and J. Dual, "Manipulation of micrometer sized particles within a micromachined fluidic device to form two-dimensional patterns using ultrasound," *The Journal of the Acoustical Society of America*, vol. 121, no. 2, pp. 778–785, 2007.

[6] C. Courtney, C.-K. Ong, B. Drinkwater, A. Bernassau, P. Wilcox, and D. Cumming, "Manipulation of particles in two dimensions using phase controllable ultrasonic standing waves," *Proceedings of the Royal Society A: Mathematical, Physical and Engineering Science.*, 2011.

[7] A. Bernassau, F. Gesellchen, P. MacPherson, M. Riehle, and D. Cumming, "Direct patterning of mammalian cells in an ultrasonic heptagon stencil," *Biomedical Microdevices*, vol. 14, no. 3, pp. 559–564, 2012.

[8] A. Bernassau, C.-K. Ong, Y. Ma, P. MacPherson, C. Courtney, M. Riehle, B. Drinkwater, and D. Cumming, "Two-dimensional manipulation of micro particles by acoustic radiation pressure in a heptagon cell," *Ultrasonics, Ferroelectrics and Frequency Control, IEEE Transactions on*, vol. 58, no. 10, pp. 2132–2138, 2011.

[9] X. Ding, S.-C. Lin, B. Kiraly, H. Yue, L. S, I.-K. Chiang, J. Shi, S. Benkovic, and T. Huang, "On-chip manipulation of single microparticles, cells, and organisms using surface acoustic waves," *Proceedings of the National Academy of Sciences*, vol. 109, no. 28, pp. 11 105–11 109, 2012.

[10] P. Glynne-Jones, C. Demore, Y. Congwei, Q. Yongqiang, S. Cochran, and M. Hill, "Array-controlled ultrasonic manipulation of particles in planar acoustic resonator," *Ultrasonics, Ferroelectrics, and Frequency Control, IEEE Transactions on*, vol. 59, no. 6, pp. 1258–1266, June 2012.

[11] C. Courtney, C. Demore, H. Wu, A. Grinenko, P. Wilcox, S. Cochran, and B. Drinkwater, "Independent trapping and manipulation of microparticles using dexterous acoustic tweezers," *Applied Physics Letters*, vol. 104, no. 15, 2014.

[12] M. Saito, T. Daian, K. Hayashi, and S.-Y. Izumida, "Fabrication of a polymer composite with periodic structure by the use of ultrasonic waves," *Journal of Applied Physics*, vol. 83, no. 7, pp. 3490–3494, 1998.

[13] M. Saito and Y. Imanishi, "Host-guest composites containing ultrasonically arranged particles," *Journal of Materials Science*, vol. 35, no. 10, pp. 2373–2377, 2000.

[14] Y. Cao, W. Xie, J. Sun, B. Wei, and S. Lin, "Preparation of epoxy blends with nanoparticles by acoustic levitation technique," *Journal of Applied Polymer Science*, vol. 86, no. 1, pp. 84–89, 2002.

[15] L. Gherardini, C. Cousins, J. Hawkes, J. Spengler, S. Radel, H. Lawler, B. Devcic-Kuhar, M. Gröschl, W. Coakley, and A. McLoughlin, "A new immobilisation method to arrange particles in a gel matrix by ultrasound standing waves," *Ultrasound in Medicine & Biology*, vol. 31, no. 2, pp. 261–272, 2005.

[16] T. Tuziuti, Y. Masuda, K. Yasui, and K. Kato, "Two-dimensional patterning of inorganic particles in resin using ultrasound-induced plate

vibration," *Japanese Journal of Applied Physics*, vol. 50, no. 8, p. 088006, 2011.
[17] Y. Chen, X. Ding, S.-C. Lin, S. Yang, P.-H. Huang, N. Nama, Y. Zhao, A. Nawaz, F. Guo, W. Wang, Y. Gu, T. Mallouk, and T. Huang, "Tunable nanowire patterning using standing surface acoustic waves," *ACS Nano*, vol. 7, no. 4, pp. 3306–3314, 2013.
[18] M.-S. Scholz, B. Drinkwater, and R. Trask, "Ultrasonic assembly of anisotropic short fibre reinforced composites," *Ultrasonics*, vol. 54, no. 4, pp. 1015–1019, 2014.
[19] ——, "Ultrasonic assembly of short fibre reinforced composites," in *Ultrasonics Symposium (IUS), 2014 IEEE International*, 2014, pp. 369–372.
[20] F. Mitri, F. Garzon, and D. Sinha, "Characterization of acoustically engineered polymer nanocomposite metamaterials using x-ray micro-computed tomography," *Review of Scientific Instruments*, vol. 82, no. 3, 2011.
[21] M. Caleap and B. Drinkwater, "Acoustically trapped colloidal crystals that are reconfigurable in real time," *Proceedings of the National Academy of Sciences*, vol. 111, no. 17, pp. 6226–6230, 2014.
[22] A. Toepler, *Beobachtungen nach einer neuen optischen Methode: Ein Beitrag zur Experimental-Physik*. Cohen, 1864.
[23] T. Pullawan, A. Wilkinson, and S. Eichhorn, "Influence of magnetic field alignment of cellulose whiskers on the mechanics of all-cellulose nanocomposites," *Biomacromolecules*, vol. 13, no. 8, pp. 2528–2536, 2012.
[24] S. Rogers, T. Waigh, X. Zhao, and J. Lu, "Precise particle tracking against a complicated background: polynomial fitting with gaussian weight," *Physical Biology*, vol. 4, no. 3, p. 220, 2007.
[25] D. Leedom, R. Krimholtz, and G. Matthaei, "Equivalent circuits for transducers having arbitrary even- or odd-symmetry piezoelectric excitation," *Sonics and Ultrasonics, IEEE Transactions on*, vol. 18, no. 3, pp. 128–141, 1971.
[26] P. Wilcox, R. Monkhouse, P. Cawley, M. Lowe, and B. Auld, "Development of a computer model for an ultrasonic polymer film transducer system," *NDT & E International*, vol. 31, no. 1, pp. 51–64, 1998.
[27] M. Hill, "The selection of layer thicknesses to control acoustic radiation force profiles in layered resonators," *The Journal of the Acoustical Society of America*, vol. 114, no. 5, pp. 2654–2661, 2003.
[28] COMSOL Multiphysics, "COMSOL Multiphysics user's guide, v4.3," 2012.
[29] J. Slotwinski, *Handbook of Reference Data for NonDestructive Testing*, ser. DS68, L. Mordfin, Ed. ASTM International, 2002. [Online]. Available: http://compass.astm.org/download/DS68-EB.21338.pdf
[30] Noliac Group, "Piezo materials specification," http://www.noliac.com/Specification-141.aspx, August 2014.
[31] W. Callister and D. Rethwisch, *Materials Science and Engineering*, 8th ed. John Wiley & Sons (Asia) Pte Ltd, 2011.
[32] MathWorks, "Fourier series," http://uk.mathworks.com/help/curvefit/fourier.html#bs1rmk5, March 2015.
[33] L. Gor'kov, "On the forces acting on a small particle in an acoustical field in an ideal fluid," *Soviet Physics Doklady*, vol. 6, p. 773, 1962.